RSC Advances

PAPER

View Article Online
View Journal | View Issue

Cite this: *RSC Adv.*, 2014, **4**, 62115

Fast and simplified synthesis of cuprous oxide nanoparticles: annealing studies and photocatalytic activity†

Liangbin Xiong,*[ab] Huaqing Xiao,[a] Shunsheng Chen,[c] Zhihong Chen,[a] Xunong Yi,[a] Sheng Wen,[d] Genwen Zheng,[d] Yaoming Ding[a] and Huaqing Yu*[a]

Received 15th October 2014
Accepted 6th November 2014

DOI: 10.1039/c4ra12406e

www.rsc.org/advances

We synthesized highly (111) plane-oriented cuprous oxide (Cu_2O) nanoparticles (NPs) by a fast and simplified chemical deposition method using an inorganic process at ambient temperature. The variations of crystal structure parameters, morphology, energy bands, and Brunauer–Emmett–Teller (BET) surface areas were recorded for Cu_2O NPs at different annealing temperatures under N_2 atmosphere. A phase coexistence of Cu_2O and Cu was observed after the Cu_2O NPs was annealed at 600 °C for 2 h under N_2 atmosphere. The Cu_2O NPs show high BET surface areas and a blue shift of absorption edge in comparison with Cu_2O microparticles. We observed a superior photocatalytic activity for the degradation of methyl orange (MO) by Cu_2O NPs, which reached 100% in 55 min with as high as 7.26 mg min^{-1} g^{-1} of decolorization rate. However, Cu_2O NPs are more vulnerable to photocorrosion than Cu_2O microparticles. The mechanisms of photocatalysis for Cu_2O under visible light were also discussed in detail. Hydrogen peroxide and hydroxyl radicals were found responsible for the decolorization of MO.

1. Introduction

Cuprous oxide (Cu_2O) nanoparticles (NPs) are widely used as antiseptic, germicide, catalyst and colorant in daily life.[1,2] They are also a promising material for photoelectric transition,[3,4] lithium ion cell cathode,[5] and photon sensing.[6] In recent years, Cu_2O NPs have been found to be a stable photocatalyst particularly applied to hydrogen generation[7,8] and the degradation of organic contamination under visible light (VL).[9] Thus, the synthesis of Cu_2O NPs is highly interesting not only for the further development of synthetic strategies, but also for the examination of their properties.

Various preparation methods for Cu_2O NPs[10–15] have been developed. In these methods for forming Cu_2O NPs, organic compounds are frequently used as the precursor[15] or as surfactant and template for preventing aggregation and controlling size as well as morphology.[10–14] However, the use of organics often inhibits the progress of photocatalytic (PC) reactions due to the covering of Cu_2O by the surfactant.[16] Furthermore, Cu_2O NPs with highly ordered nanostructures have attracted much attention in recent years due to their novel properties in photocatalysis and their stability. The (111) plane of Cu_2O was found to show superior PC activity,[17,18] and Cu_2O exposing (111) facets can be used as a stable photocatalyst.[19–21] Therefore, the fabrication of Cu_2O NPs with preferentially oriented (111) facets by using inorganic precursors has become an important issue.

Recently, we reported the chemical synthesis of Cu_2O films with periodic pattern transfer by using a chemical bath deposition technology (at 65 °C).[22] In the present work, this deposition technology was improved, and a fast and simplified synthesis of Cu_2O NPs with preferentially oriented (111) facets was successfully achieved at ambient temperature without high energy demand, complicated apparatus, or any organic compounds and surfactants. Particularly, we attempted to investigate the effect of heating Cu_2O under inert atmosphere on its morphology, optical properties, stability and PC activity, since no study has been carried out on this so far, and heating Cu_2O in air could cause a conversion of Cu_2O to CuO.[23–25] Finally, the behaviors of adsorption, photocatalysis and stability

[a]*School of Physics and Electronic-Information Engineering, Hubei Engineering University, Xiaogan, 432000, China. E-mail: Xiong_lb@yahoo.com; yuhuaqing@126.com; Tel: +86-712-234-5441*

[b]*Key Laboratory of Artificial Micro- and Nano-structures of Ministry of Education of China, School of Physics & Technology, Wuhan University, Wuhan, Hubei 430072, China*

[c]*The Institute for Quantum Materials, School of Mathematics and Physics, Hubei Polytechnic University, Huangshi, 435003, China*

[d]*College of Chemistry and Materials Science, Hubei Engineering University, Xiaogan 432000, China*

† Electronic supplementary information (ESI) available: Photographs of samples 2–5, the peak height/area ratio of planes (111) and (200) of samples 1–5, the UV-vis diffuse reflectance spectra for samples 1, 3, 4 and their corresponding $(\alpha E_p)^2$ *vs.* E_p curves, and XRD patterns of samples 2–5 before and after PC experiments are provided as in ESI. See DOI: 10.1039/c4ra12406e

of unannealed and annealed Cu_2O were investigated, and the mechanisms of Cu_2O for PC degradation of methyl orange (MO) under VL are discussed in detail.

2. Experimental section

2.1 Materials

Copper(II) sulfate ($CuSO_4 \cdot 5H_2O$, 98.0% purity), sodium thiosulfate ($Na_2S_2O_3$, 99.0% purity), sodium hydroxide (NaOH, 99% purity) and MO (85% purity) were obtained from Sinopharm (China) and used as purchased. 2,3-Bis(2-methoxy-4-nitro-5-sulfophehyl)-2*H*-tetrazolium-5-carboxanilide (XTT) (>98% purity), terephthalic acid (TA) (98% purity), horseradish peroxidase (POD) (activity: 250–330 units per mg solid), and *N*,*N*-diethyl-*p*-phenylenediamine (DPD) (97% purity) were received from Sigma-Aldrich and used without further purification. The solutions used in this work were prepared with deionized water further purified with a Millipore Milli-Q (Millipore, Bedford, MA, USA) purification system (resistivity $\geq$ 18.2 MΩ).

2.2 Synthesis of Cu_2O NPs

A colorless 500 mL stock solution of the Cu_2O NP mixture was prepared by adding 400 mL of 1 M $Na_2S_2O_3$ to 100 mL of 1 M $CuSO_4$ solution. The same volume (500 mL) of 1 M NaOH solution was placed in another beaker. The mixture was poured into the 1 M NaOH solution with vigorous stirring. The Cu_2O powder was obtained by centrifugation and dried. Subsequently, the Cu_2O powder was divided into six equal parts, five of which were annealed at 200, 300, 400, 500 and 600 °C in N_2 atmosphere with a flow rate of 35 sccm. The unannealed Cu_2O powder and those annealed at 200, 300, 400, 500 and 600 °C were named sample 1, 2, 3, 4, 5, and 6, respectively.

2.3 Characterization

The phase purity of all samples was characterized by X-ray powder diffraction (XRD) using an X-ray diffractometer (Y-2000) with Cu Kα radiation (λ = 1.5418 Å). A scan efficiency of 0.1° S^{-1} was applied to record the powder patterns in the range of $20° \leq 2\theta \leq 80°$. Scanning electron microscopy (SEM) images were obtained on a JEOL SM-6700F microscope operated at 5 kV. X-ray photoelectron spectroscopy (XPS) analyses were performed on a PHI-1600 ESCA spectrometer (USA) using 300 W Mg Kα radiation, and the binding energies were referenced to the C1s line at 285 eV of adventitious carbon. Transmission electron microscopy (TEM) and high-resolution transmission electron microscopy (HRTEM) were carried out with JEOL JEM-100CXII. The Brunauer–Emmett–Teller (BET) surface areas of the samples were determined by a high-speed automated area and pore size analyzer (NOVA 2000e).

2.4 Adsorption and PC activity measurement

The liquid phase degradation of MO was used as a model reaction to evaluate the PC activity of the Cu_2O powder. In a typical PC experiment, 0.1 g catalyst was dispersed in 400 mL of 100 mg L^{-1} MO solution. Prior to irradiation, the suspension was then sonicated for 30 min in the dark to ensure good dispersion of the catalyst solution and the establishment of adsorption/desorption equilibrium of the dye onto the photocatalyst surface. PC reactions were conducted in a cylindrical quartz reactor with water circulation to keep the reaction temperature of 25 °C. The equilibrium dye concentration was used as the initial concentration of the dye solution to calculate degradation efficiency. Subsequently, the suspension was transferred to the reactor. A 300 W xenon lamp (Shanghai Lansheng Ltd., Shanghai) was used as a visible light source. A UV cutoff filter (λ < 400 nm) was used to ensure VL irradiation. The light intensity was measured by a light meter (LI-COR, USA), and the light intensity for the experiments was fixed at 1800 mW cm^{-2}. Aeration was performed by an air pump to ensure a constant supply of oxygen and to accomplish stirring the solution with the photocatalyst during photoreaction. At given irradiation time intervals, a 5 mL liquor was sampled and centrifuged at 4500 rpm for 15 min to remove the photocatalyst. The MO concentration was analyzed by recording variations of the absorption band maximum at 465 nm (defined as A_t) in the UV-vis spectra of MO by using a UV-vis spectrophotometer (UV-1700, SHIMADZU). The adsorption extent R_a of MO on the photocatalyst was determined by the difference in MO concentration between the original solution (defined as A_0) and the filtrate of the MO/photocatalyst suspensions (defined as A_0'). The adsorption extent R_a of the dye on the photocatalyst was $R_a = (A_0 - A_0')/A_0 \times 100\%$. The degradation efficiency (R_d) of MO was calculated by the following equation: $R_d = (A_0' - A_t)/A_0' \times 100\%$. The PC activity of all Cu_2O samples was detected by this method. In addition, the decolorization rates were also calculated according to following equation: $R_{dec} = V_0C_0/Q_0T \times 100\%$ (unit: mg min^{-1} g^{-1}), where R_{dec} is the decolorization rate, and V_0, C_0, Q_0, and T are the volume of suspension with MO and catalyst, the initial concentration of MO, the amount of catalyst, and the time for PC reaction, respectively. Thus, here, decolorization rate is used to characterize how much dye can be discolored by a given amount of catalyst in a given time. We did this in an attempt to have a rough comparison between the PC activity of as-prepared Cu_2O and that reported in publications.

2.5 Measurement of hydroxyl, hydrogen peroxide and superoxide radicals

Hydroxyl radical (•OH) was detected by a photoluminescence (PL) method using TA as a probe molecule.[26] TA readily reacts with •OH to produce a highly fluorescent product, 2-hydroxy-TA (TA-•OH), which was measured by an Infinite M200 fluorescence spectrophotometer (Tecan, Switzerland) at 425 nm emission wavelength and 315 nm excitation wavelength. The experimental procedure is similar to the PC measurement, except that the aqueous MO solution was replaced with 4×10^{-4} M TA and 2×10^{-3} M NaOH.

Superoxide radical ($\cdot O_2^-$) was measured by XTT,[27] which can be reduced by $\cdot O_2^-$ to form XTT-formazan. The formazan has an absorption spectrum (measured by UV-1700, SHIMADZU) with a peak at 470 nm that can be used to quantify the relative amount of $\cdot O_2^-$ present. The experimental procedure is similar to the PC

measurement, except that the MO was replaced with 1×10^{-4} M XTT.

H_2O_2 was analyzed photometrically by the POD-catalyzed oxidation product of DPD,[28,29] which was measured by UV/vis spectrophotometer (UV-1700, SHIMADZU) at 551 nm. The experimental procedure is as follows: (1) 0.3 mL of phosphate buffer (0.5 M Na_2HPO_4 and NaH_2PO_4) was added to 2.7 mL of water/sample in cuvette and mixed; (2) 50 μL of DPD reagent and 50 μL of POD reagent were added in rapid succession and mixed for 10 s; (3) the absorption spectrum at 500–620 nm of the solution was taken. Water with the addition of buffer and DPD reagent was used as blank.

3. Results and discussion

3.1 Characterization of Cu_2O

Cu_2O NPs were synthesized through the reduction of blue copperas ($CuSO_4 \cdot 5H_2O$) by $Na_2S_2O_3$ as the reducing agent at ambient temperature in an alkaline aqueous solution. A colorless solution of copper thiosulfate complex was formed after an overdose of $Na_2S_2O_3$ solution was added into the blue copperas solution by the following complexation equilibrium:

$$2Cu^{2+} + 4S_2O_3^{2-} \rightarrow 2[CuS_2O_3]^- + [S_4O_6]^{2-} \quad (1)$$

In the copper thiosulfate complex solution, free Cu^+ ions were formed by the dissociation equilibrium:[30]

$$[CuS_2O_3]^- \rightarrow Cu^+ + S_2O_3^{2-} \quad (2)$$

After the copper thiosulfate complex solution was poured into the NaOH solution, a yellow precipitate appeared almost simultaneously, suggesting the generation of Cu_2O. The formation of the precipitate could be simply expressed as the reaction of free Cu^+ ions with OH^- ions:

$$2Cu^+ + OH^- \rightarrow Cu_2O + H^+ \quad (3)$$

Fig. 1a shows the XRD spectra obtained *in situ* for samples 1–5. Five peaks at $2\theta = 29.78°$, 36.56°, 42.39°, 62.51° and 73.46° could be indexed to the (110), (111), (200), (220) and (311) planes of the Cu_2O cubic phase with lattice constant $\alpha = 0.4266$ nm, which is very close to the values in JCPDS-International Centre for Diffraction Data (PDF, Powder Diffraction File, no. 05-0667, 1996). The XRD spectrum of sample 1 (unannealed Cu_2O) is as good as that of sample 2, indicating that heating Cu_2O at 200 °C under N_2 atmosphere did not change its phase composition. No other peaks suggesting impurities, or significant changes in the peak locations of the XRD spectra, were detected after the heat treatments, indicating that pure Cu_2O powders were obtained under current synthetic conditions.

It can also be seen from Fig. 1a that as the annealing temperature increases, so does the intensity of all of the diffraction peaks, but their full width at half maximum (FWHM) decreases. It is well known that the width of the diffraction peak increases with the decreasing size of crystalline grain. The relationship of the diffraction peak FWHM ($\Delta(2\theta)$) and the size of crystalline grain (D) can be expressed as the Debye–Scherrer

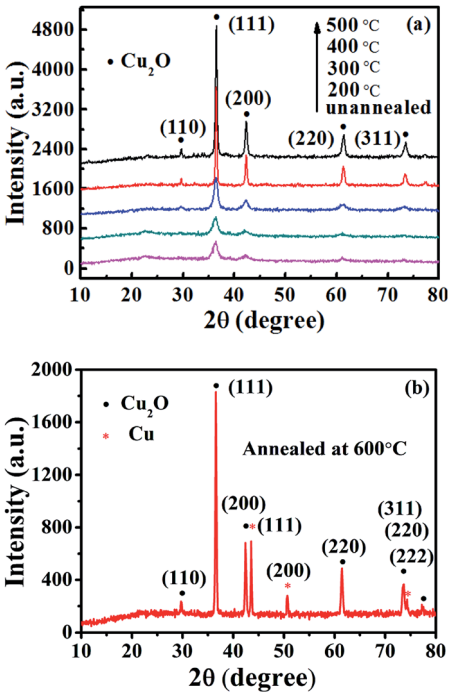

Fig. 1 XRD patterns of (a) Cu_2O NPs annealed at 200, 300, 400 and 500 °C; (b) 600 °C in N_2 atmosphere for 2 h.

formula: $D = 0.89\lambda/\Delta(2\theta)\cos\theta$, where λ is the wavelength of the X-ray diffractometer incident ray (Cu Kα, $\lambda = 1.5418$ Å). Thus, according to the FWHM of the diffraction peaks of the (111) plane of Cu_2O, the average Cu_2O crystal sizes for samples 1–5 can be estimated as 7.73 nm, 7.73 nm, 9.39 nm, 21.91 nm, and 26.29 nm, respectively, indicating that the crystallinity of Cu_2O increased with increasing annealing temperature. The heat-induced growth of Cu_2O crystallite contributes to the increase of crystallinity, because higher ordering in the structure of Cu_2O makes the X-ray peak sharper and narrower. The peak at 36.56° was always dominant in all the annealing temperatures, indicating that these Cu_2O samples have highly oriented (111) planes. The numerical information of the peak height/area ratio of planes (111) and (200) for samples 1–5 are provided in Table S1.† A gradually increasing peak height/area ratio of the (111) plane indicates the formation of more highly oriented (111) planes with increasing annealing temperature. The formation of Cu_2O NPs highly oriented to the (111) plane was also confirmed by the examination of HRTEM and the corresponding selected-area electron diffraction (SED) pattern. Fig. 2a indicates the Cu_2O NPs were composed of rod-like and sphere-like nanostructures. One Cu_2O nanorod in the square area in Fig. 2a was enlarged and shown in Fig. 2b, in which the non-uniform contrast of the image indicates nanocrystalline particles with diameters of about 5–10 nm in the nanorods. The interplanar spacing of the lattice fringes in the HRTEM image of the Cu_2O nanorod (Fig. 2b) is about 0.2412 nm, which corresponds to the (111) plane of the Cu_2O NPs.[22] The brighter circle corresponds more to the (111) plane than the others in the SED

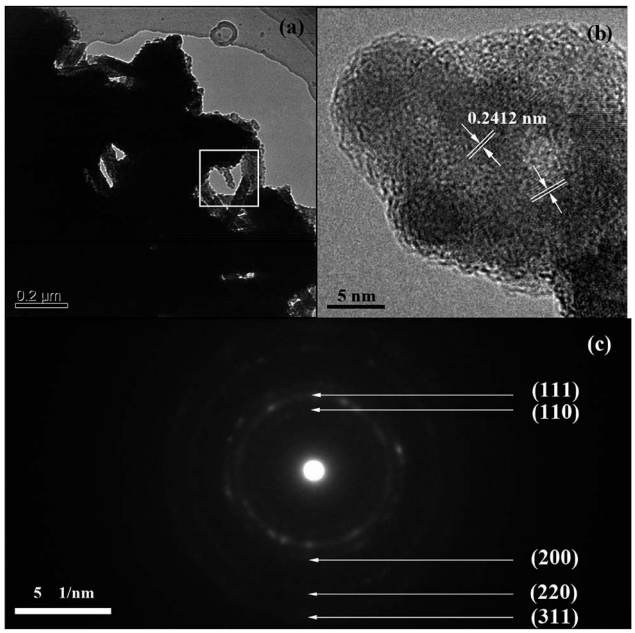

Fig. 2 (a) TEM, (b) HRTEM images and (c) selected-area electron diffraction pattern corresponding to the whole-image (b) area for unannealed Cu_2O NPs.

pattern (Fig. 2c) of the whole image (Fig. 2b), also indicating the formation of Cu_2O NPs highly oriented to the (111) plane.

Fig. 3 records a representative panoramic view of samples 2–5, from which the variation of morphology of Cu_2O with the annealing temperatures is observed. The SEM image of sample 1 is similar to that of sample 2 (not shown here), indicating that the morphology of Cu_2O did not change when annealed at 200 °C. The result is in good agreement with our XRD data and the report by Paracchino, *et al.* that heating Cu_2O to 250 °C in N_2 atmosphere did not change the morphology of the film.[23] However, as the annealing temperature increased, Cu_2O NPs with rod-like and sphere-like nanostructures disappeared, and the original Cu_2O NPs grew into large architectures with sizes ranging from several hundred nanometers to several micrometers (Fig. 3a–d and a′–d′), suggesting that annealing over 300 °C significantly influences the morphology and size of Cu_2O. Interestingly, when Cu_2O NPs were annealed at 600 °C, a phase coexistence of Cu_2O and Cu was observed due to the appearance of four additional peaks at $2\theta = 43.2°$, 50.4° and 74.1° corresponding to the (111), (200) and (220) planes of copper (JCPDS card no. 04-0836)[31] and the other one at 77.25° corresponding to the (222) plane of Cu_2O (Fig. 1b). The heat treatment in N_2 atmosphere at 600 °C therefore caused the decomposition of Cu_2O (eqn (4)).

$$2Cu_2O \rightarrow Cu + O_2 \quad (4)$$

3.2 Optical property of Cu_2O

Fig. 4a shows the optical absorption spectra for samples 2 and 5. To estimate the optical absorption edges for these two samples,

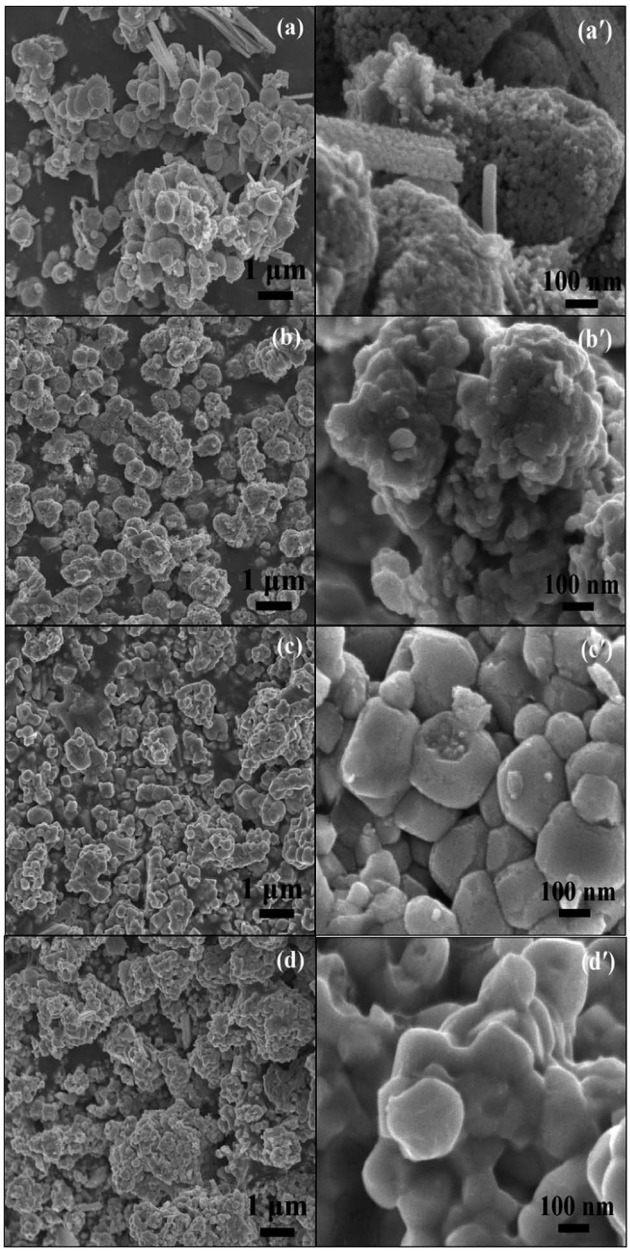

Fig. 3 SEM images of Cu_2O NPs annealed at (a) 200, (b) 300, (c) 400 and (d) 500 °C and their enlarged images (a′), (b′), (c′), and (d′), respectively.

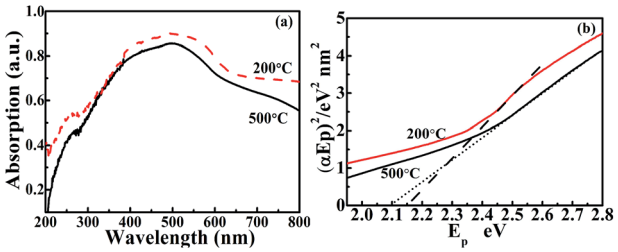

Fig. 4 (a) The UV-vis diffuse reflectance spectra for Cu_2O NPs annealed at 200 and 500 °C and (b) their corresponding $(\alpha E_p)^2$ *vs.* E_p curves, respectively.

Table 1 The crystal size, band gap, BET surface area, color, adsorption extent (R_a), and decolorization rates of unannealed Cu_2O NPs and Cu_2O NPs annealed at 200, 300, 400 and 500 °C

Samples	1	2	3	4	5
BET surface area ($m^2\ g^{-1}$)	21.63	21.37	6.156	5.521	3.011
Crystal size (111) (nm)	7.73	7.73	9.39	21.91	26.29
Band gap (eV)	2.15	2.15	2.12	2.11	2.10
Color	Dark yellow	Dark yellow	Yellow	Light orange	Orange
Adsorption extent (R_a)	39.1%	38.4%	11.4%	9.6%	5.7%
Decolorization rate (R_{dec})[a]	7.26	6.67	3.27	2.77	1.70

[a] The unit of decolorization rate is mg min^{-1} g^{-1}. The time for calculating decolorization rates for samples 1–5 are 55, 60, 120, 120 and 120 min, respectively. The decolorization rate is an overall averaged rate for each sample in a given time.

$(\alpha h\nu)^{1/n}$ *versus* $h\nu$ curves were plotted (Fig. 4b) for n values ($n = 1/2$), a direct optical transition.[32] Here, α is the optical absorption coefficient calculated from the absorption spectra, and h is the incident photon energy. The band gaps estimated for samples 2 and 5 are 2.15 and 2.10 eV, respectively, which are in agreement with the literature value of 2.1 eV for Cu_2O bulk crystal.[33] The absorption edge wavelengths for samples 2 and 5 were estimated to be 577 and 590 nm according to their band baps, respectively, indicating a substantial red shift for the absorption of sample 5 in comparison with that of sample 2. The UV-vis diffuse reflectance spectra and their corresponding $(\alpha E_p)^2$ *vs.* E_p curves for samples 1, 3 and 4 are given in Fig. S2.† The band gaps of samples 1, 3 and 4 were also calculated by the same method (see Table 1). The studies indicate that the band gaps of Cu_2O NPs decrease with increasing annealing temperature. We observed that the colors of samples 2–5 generally changed from dark yellow to orange (see Table 1 and Fig. S1 in ESI†), also suggesting the variation of optical absorption with different annealing temperatures.

3.3 PC activity of Cu_2O

The adsorption extent (R_a) and decolorization ratio, as well as the MO degradation efficiency of the Cu_2O samples are given in Table 1 and Fig. 5, respectively. Samples 1 and 2 show a close adsorption extent, decolorization rate and degradation efficiency, indicating that annealing treatment for Cu_2O NPs at 200 °C did not significantly affect its adsorption and PC activity towards MO. However, as the annealing temperature increased, these Cu_2O samples showed a diminishing adsorption extent and PC activity. The much higher degradation efficiency of samples 1 and 2 compared to other Cu_2O samples may be ascribed to their small particle sizes, which can increase their adsorption ability and thereby improve their PC activity. Moreover, the small photocatalyst size can result in more efficient transfer of photogenerated charges to the surface, also contributing to the efficient PC reaction, whereas the aggregation of photocatalyst particles involved a decrease in specific surface area as well as a change in the light scattering property of the particles,[34] resulting in the degradation of PC efficiency.[35] Moreover, the higher decolorization rates of samples 1 (7.26 mg min^{-1} g^{-1}) and 2 (6.67 mg min^{-1} g^{-1}) (see Table 1) than the reported values of 6,[36] 2.75 (ref. 37) and 0.238 (ref. 12) mg min^{-1} g^{-1} further indicate the superior PC activity of Cu_2O NPs towards MO.

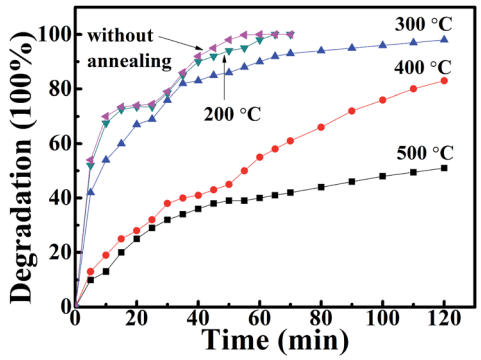

Fig. 5 Degradation efficiencies of MO for unannealed Cu_2O NPs and Cu_2O NPs annealed at 200, 300, 400 and 500 °C under VL. 0.1 g catalyst was dispersed in 300 mL of 100 mg L^{-1} MO solution.

3.4 Stability of Cu_2O

The stability of the Cu_2O samples was investigated by comparing the structures and valence states of the Cu_2O samples before and after PC experiments. Fig. S3† shows XRD patterns of samples 2–5 before and after PC experiments. The XRD pattern of sample 1 is similar to that of sample 2 after PC experiment (not shown here). Two new peaks at $2\theta = 38.73°$ and 48.65°, corresponding to the (111) and (202) planes of tenorite phase CuO (PDF, Powder Diffraction File, no. 02-1040), appeared in the XRD patterns of both samples 2 and 3, indicating that they were partly oxidized into CuO during the PC process. However, no obvious change could be observed for the XRD patterns of samples 4 and 5, indicating that annealing at a higher temperature contributed to a better stability for Cu_2O.

XPS spectra were recorded to monitor the valence states of the Cu_2O samples before and after PC experiments. Fig. 6a shows a representative XPS spectrum for samples 1–5 before PC experiments. It is hard to simulate the peak, because it is not so broad, and there is no shoulder peak. The binding energy of Cu2p (932.9 eV) is the same as the standard binding energy of Cu2p in Cu_2O, indicating that samples 1–5 were prepared as pure Cu_2O, which is well in agreement with the XRD data. Fig. 6b and c show the XPS spectra of sample 1 and sample 5

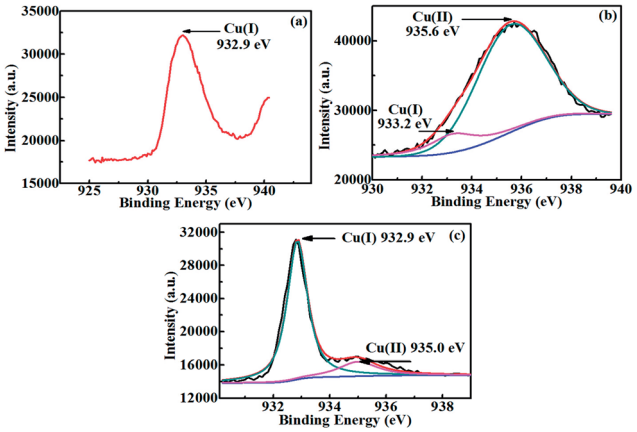

Fig. 6 (a) Representative XPS spectrum of samples 1–5 before PC experiments; XPS spectra of (b) sample 1 and (c) sample 5 after PC experiments.

after PC experiments, respectively. The XPS spectra of samples 2, 3 and 4 after PC experiments were similar to those shown in Fig. 6b and c, respectively. All the similar data are not shown here. XPS spectra of both Fig. 6b and c show a broad peak simulated with the Gaussian equation, which leads to two split peaks. According to the cited publication,[38] the $Cu2p_{3/2}$ level of Cu_2O is narrow (FWHM = 2.0 ± 0.1 eV) and has a binding energy of 933.05 ± 0.75 eV, while that of CuO is broad (FWHM = 2.85 ± 0.25 eV), with a binding energy of 935.2 ± 0.35 eV. A detailed description of the binding energies, FWHM and relative contents of the different peaks for sample 1 and sample 5 after the PC experiments are listed in Table 2.

It can be seen form Table 2 that both samples 1 and 5, after PC experiments, have two kinds of surface states, Cu^+ and Cu^{2+}. The ratio of the area of the peaks denotes the relative amounts of Cu^+ to Cu^{2+} on the surface. The peak area ratio of Cu^+ to Cu^{2+} on the surface for samples 1 and 5 are 0.09 and 10.87, respectively, indicating that the Cu^{2+} is the main surface state for sample 1 (similar to samples 2 and 3), and Cu^+ is the main surface state for sample 5 (similar to sample 4) after PC experiments. The XRD spectra of samples 1–3 before and after the PC experiments also confirm the transformation of Cu_2O to CuO. However, XRD spectra of samples 4 and 5 before and after PC experiments could not identify the oxidation of Cu_2O to CuO, suggesting that the amount of CuO is too low to be detected by XRD measurement, and only a very thin surface layer of Cu_2O was oxidized into CuO for samples 4 and 5 after the PC experiments. The results further confirm that the Cu_2O annealed over 400 °C had better stability than that annealed below 400 °C.

Table 2 The binding energies, FWHM, relative contents and area ratio of different peaks of unannealed Cu_2O and Cu_2O NPs annealed at 500 °C after the PC experiments

Sample	1		5	
Peaks	Cu^+	Cu^{2+}	Cu^+	Cu^{2+}
Binding energy (eV)	933.2	935.6	932.7	934.9
FWHM	1.93	3.0	1.85	2.9
Area	7142	79 156	53 694	4939
Cu^+/Cu^{2+}	0.09		10.87	

3.5 Detection of reactive oxygen species (ROSs)

The generation of ˙OH was detected by the photoluminescence (PL) method. Usually, PL intensity is proportional to the amount of produced ˙OH in solution. A gradual increase in PL intensity of characteristic peaks at about λ = 425 nm was observed (Fig. 7a), indicating that the ˙OH was formed during the PC process. XTT is a widely used $^{\cdot}O_2^-$ probe with a high rate constant for the reaction of $^{\cdot}O_2^-$. Fig. 7b shows no absorption peak at λ = 470 nm, indicating that $^{\cdot}O_2^-$ was not produced.[27] H_2O_2 production was analyzed photometrically. Fig. 7c shows that H_2O_2 was produced; its concentration increased at first and became stable with prolonged irradiation time due to the decomposition of H_2O_2 in parallel with its production.[39]

3.6 Mechanisms of photocatalysis

The general principle of photocatalysis is that when illuminated by light with photoenergy greater than the band gap, the electrons (e^-) of NPs are promoted across the band gap to the conduction band, which creates a hole (h^+) in the valence band. Electrons in the conduction band and holes in the valence band exhibit high reducing and oxidizing power, respectively. The electron can react with molecular oxygen to produce $^{\cdot}O_2^-$ through a reductive process. Although $^{\cdot}O_2^-$ is not a strong oxidant, it has significant PC implications as a precursor for H_2O_2 and ˙OH.[27] The hole can abstract electrons from water and/or hydroxyl ions to generate ˙OH through an oxidative

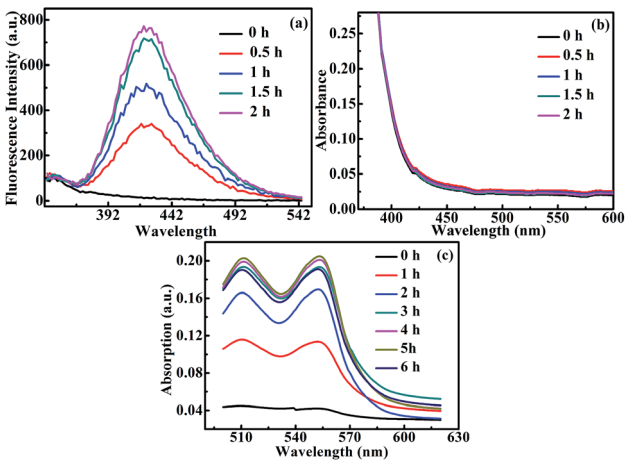

Fig. 7 (a) Fluorescence emission spectral changes for the filtrate from the suspension of unannealed Cu_2O with 4×10^{-4} M TA and 2×10^{-3} M NaOH at different irradiation times (emission at 425 nm, excitation at 315 nm); (b) absorption spectral changes for the filtrate from the suspension with unannealed Cu_2O and 1×10^{-4} M XTT at different irradiation times (absorption peak 470 nm); (c) absorption spectra of the DPD/POD reagent after reaction with H_2O_2 (absorption peak 551 nm).

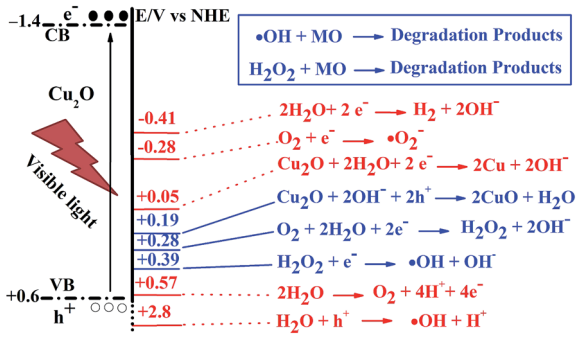

Fig. 8 Energy level diagram of Cu_2O and the events possibly occurring during the PC process.

process.[27] Thus, h^+, $^{\cdot}OH$, H_2O_2 and $^{\cdot}O_2^-$ are considered to be the major reactive species for PC dye decolorization.[40]

Fig. 8 shows the energy level diagram of Cu_2O as well as the events possibly occurring during the PC process. An examination of the band structure of Cu_2O in Fig. 8 leads to the conclusion that the redox potentials for H_2, $^{\cdot}O_2^-$, O_2 and H_2O_2 evolution, the oxidation of Cu_2O to CuO and the reduction of Cu_2O to Cu are all within the band gap, and therefore, all of these processes are possible, in principle. However, not all the reactions are kinetically favorable; for example, the driving force for water oxidation is minimal, while the oxidation of Cu_2O is thermodynamically favorable.[21] Thus, we have to identify which reactions are available both kinetically and thermodynamically take place according to the experimental results. Then, we can further analyze the roles of the electron, hole, and ROSs for the PC process.

Cu_2O is one of the semiconductors with the highest conduction bands. The band gap of Cu_2O NPs was determined as 2.02 eV in this work, and the potential of its conduction band is −1.4 V (*vs.* NHE, the same below).[41] When Cu_2O NPs are irradiated by VL, electrons are separated from holes (eqn (5)).

$$Cu_2O + h\nu \rightarrow Cu_2O\,(e^-) + Cu_2O\,(h^+) \quad (5)$$

Thus, those photogenerated electrons with high energy in the conduction band of Cu_2O, besides recombining with holes (eqn (6)) or reducing Cu_2O to Cu (which happens at +0.05 V, eqn (7)),[21] are likely to transfer to the surface of Cu_2O to react with molecular oxygen and produce $^{\cdot}O_2^-$, H_2O_2 and $^{\cdot}OH$.

$$Cu_2O\,(e^-) + Cu_2O\,(h^+) \rightarrow \text{heat} \quad (6)$$

$$Cu_2O + 2H_2O + 2e^- \rightarrow 2Cu + 2OH^- \quad (7)$$

However, the reduction of Cu_2O to Cu by photogenerated electrons was unlikely to occur, according to our XPS data. Photogenerated electrons also were unlikely to react with molecular oxygen to produce $^{\cdot}O_2^-$ (eqn (8)), because $^{\cdot}O_2^-$ was not detected during our PC experiments.

$$O_2 + e^- \rightarrow {}^{\cdot}O_2^- \quad (8)$$

As for the hole, which is produced at about +0.6 V potential, no overpotential is available for the oxidation of water (about +0.57 V, eqn (9)).[42] It also cannot oxidize H_2O and OH^- to form H_2O_2 (+1.763 V) and $^{\cdot}OH$ (about +2.8 V), respectively. However, the oxidation of Cu_2O by the hole is favorable (+0.19 V, eqn (10)),[43] which is supported by our XRD and XPS data before and after the PC experiments.

$$2H_2O \rightarrow O_2 + 4H^+ + 4e^- \quad (9)$$

$$Cu_2O + 2OH^- + 2h^+ \rightarrow 2CuO + H_2O \quad (10)$$

Since H_2O_2 and $^{\cdot}OH$ signals were detected in our PC process, and the hole is not their origin, electrons should be responsible for the production of both H_2O_2 and $^{\cdot}OH$ by possible reductive reaction processes. The reductive reaction for the production of H_2O_2 can proceed as the cited publication[44] reported: the photogenerated electron is likely to react with molecular oxygen to produce superoxide anion ($^{\cdot}O_2^-$, −0.28 V, eqn (8)),[12] then H_2O_2 through a reductive process. However, no $^{\cdot}O_2^-$ signal was detected in our experiments, so the H_2O_2 came from the direct reduction of O_2 (+0.28 V, eqn (11)), which was more thermodynamically available.[2,45] H_2O_2 can discolor MO with a low degradation rate even in the dark,[46] suggesting that H_2O_2 is involved in the decolorization of MO during the PC process. Moreover, H_2O_2 is an electron capturer, which can capture photogenerated electrons and result in the evolution of $^{\cdot}OH$ according to eqn (12).[47,48]

$$O_2 + 2H_2O + 2e^- \rightarrow H_2O_2 + 2OH^- \quad (11)$$

$$H_2O_2 + e^- \rightarrow {}^{\cdot}OH + OH^- \quad (12)$$

Indeed, the process was available because the $^{\cdot}OH$ signal was detected in our PC process. $^{\cdot}OH$ is a strong and nonselective oxidant[45] that can result in the decolorization of MO. So, both H_2O_2 and $^{\cdot}OH$ are responsible for the degradation of MO during the PC process.

4. Conclusions

A fast and simplified synthesis of Cu_2O NPs with highly oriented (111) planes can be achieved by a chemical deposition method with an inorganic process at ambient temperature. The annealing of Cu_2O NPs shows that the higher the annealing temperature, the more highly oriented (111) planes could be formed with increasing annealing temperature. However, when heating Cu_2O at 600 °C for 2 h in N_2 atmosphere, a phase transformation occurred, and the coexistence of Cu_2O and Cu was observed. The Cu_2O NPs show high BET surface areas and a blue shift of absorption edge compared to Cu_2O microparticles. The superior PC activity of Cu_2O NPs may result from their small particle size, high BET surface areas and highly (111) plane-oriented crystal composition. However, Cu_2O NPs are more vulnerable to photocorrosion than Cu_2O microparticles. Cu_2O annealed at over 400 °C shows better stability than that annealed below 400 °C, which might be due to more highly oriented (111) planes in the Cu_2O microparticles than the

nanoparticles. H_2O_2 and $^{\bullet}OH$ played a key role for the degradation of MO during the PC process.

Acknowledgements

This work was supported by the National Natural Science Foundation of China (Grant no. 61370223 and 51303048), the Natural Science Foundation of Hubei Province (Grant no. 2014CFB579), Hubei Key Laboratory of Quality Control of Characteristic of Fruits and Vegetables, Hubei Engineering University (Grant no. 2014K11 and SWZ009), and Hubei Provincial Department of Education (Grant no. B2014025).

Notes and references

1 A. Muramatsu and T. Sugimoto, *J. Colloid Interface Sci.*, 1997, **189**, 167.
2 Y. Chen, T. W. Ng, A. Lu, Y. Li, H. Y. Yip, T. An, G. Li, H. Zhao, M. Gao and P. K. Wong, *Chem. Eng. J.*, 2013, **234**, 43.
3 C. M. Mcshane and K. S. Choi, *Phys. Chem. Chem. Phys.*, 2012, **14**, 6112.
4 C. M. Mcshane, W. P. Siripala and K.-S. Choi, *J. Phys. Chem. Lett.*, 2010, **1**, 2666.
5 J. Y. Xiang, X. L. Wang, X. H. Xia, L. Zhang, Y. Zhou, S. J. Shi and J. P. Tu, *Electrochim. Acta*, 2010, **55**, 4921.
6 S. Sahoo, S. Husale, B. Colwill, T.-M. Lu, S. Nayak and P. M. Ajayan, *ACS Nano*, 2009, **3**, 3935.
7 C. C. Hu, J. N. Nian and H. Teng, *Sol. Energy Mater. Sol. Cells*, 2008, **92**, 1071.
8 M. K. I. Senevirathna, P. K. D. D. P. Pitigala and K. Tennakone, *J. Photochem. Photobiol., A*, 2005, **171**, 257.
9 H. Yang and Z.-H. Liu, *Cryst. Growth Des.*, 2010, **10**, 2064.
10 Y. Tan, X. Xue, Q. Peng, H. Zhao, T. Wang and Y. Li, *Nano Lett.*, 2007, **7**, 3723.
11 S. Deki, K. Akamatsu, T. Yano, M. Mizuhata and A. Kajinami, *J. Mater. Chem.*, 1998, **8**, 1865.
12 L. Huang, F. Peng, H. Yu and H. Wang, *Solid State Sci.*, 2009, **11**, 129.
13 H. Liu, W. Miao, S. Yang, Z. Zhang and J. Chen, *Cryst. Growth Des.*, 2009, **9**, 1733.
14 X. Hong, G. Wang, W. Zhu, X. Shen and Y. Wang, *J. Phys. Chem. C*, 2009, **113**, 14172.
15 K. Borgohain, N. Murase and S. Mahamuni, *J. Appl. Phys.*, 2002, **92**, 1292.
16 A. J. Maira, K. L. Yeung, C. Y. Lee, P. L. Yue and C. K. Chan, *J. Catal.*, 2000, **192**, 185.
17 C. H. Kuo and M. H. Huang, *J. Am. Chem. Soc.*, 2008, **130**, 12815.
18 Y. Xu, H. Wang, Y. Yu, L. Tian, W. Zhao and B. Zhang, *J. Phys. Chem. C*, 2011, **115**, 15288.
19 Z. Zheng, B. Huang, Z. Wang, M. Guo, X. Qin, X. Zhang, P. Wang and Y. Dai, *J. Phys. Chem. C*, 2009, **113**, 14448.
20 K. L. Sowers and A. Fillinger, *J. Electrochem. Soc.*, 2009, **156**, F80.
21 L. Wu, L. Tsui, N. Swami and G. Zangari, *J. Phys. Chem. C*, 2010, **114**, 11551.
22 L. Xiong, H. Yu, G. Yang, M. Qiu, J. Chen and Y. Yu, *Thin Solid Films*, 2010, **518**, 6738.
23 A. Paracchino, N. Mathews, T. Hisatomi, M. Stefik, S. D. Tilley and M. Grätzel, *Energy Environ. Sci.*, 2012, **5**, 8673.
24 R. J. Mohd, S. M. S. Mohd, L. H. Nor and A. C. Hee, *Int. J. Electrochem. Sci.*, 2011, **6**, 6094.
25 W. Siripala, L. D. R. D. Perera, K. T. L. De Silva, J. K. D. S. Jayanetti and I. M. Dharmadasa, *Sol. Energy Mater. Sol. Cells*, 1996, **44**, 251.
26 K. Ishibashi, A. Fujishima, T. Watanabe and K. Hashimoto, *J. Photochem. Photobiol., A*, 2000, **134**, 139.
27 Y. Li, W. Zhang, J. Niu and Y. Chen, *ACS Nano*, 2012, **6**, 5164.
28 H. Bader, V. Sturzenegger and J. Hoigné, *Water Res.*, 1988, **22**, 1109.
29 W. Wang, Y. Yu, T. An, G. Li, H. Y. Yip, J. C. Yu and P. K. Wong, *Environ. Sci. Technol.*, 2012, **46**, 4599.
30 M. T. S. Nair, L. Guerrero, O. L. Arenas and P. K. Nair, *Appl. Surf. Sci.*, 1999, **150**, 143.
31 N. Yang, Z. Wang, L. Chen, Y. Wang and Y. B. Zhu, *Int. J. Refract. Met. Hard Mater.*, 2010, **28**, 198.
32 Y. Nakano, S. Saeki and T. Morikawa, *Appl. Phys. Lett.*, 2009, **94**, 022111.
33 L. Ma, J. Li, H. Sun, M. Qiu, J. Wang, J. Chen and Y. Yu, *Mater. Res. Bull.*, 2010, **45**, 961.
34 M. Yin, C. K. Wu, Y. B. Lou, C. Burda, J. T. Koberstein, Y. M. Zhu and S. O'brien, *J. Am. Chem. Soc.*, 2005, **127**, 9506.
35 C. A. Martín, M. A. Baltanás and A. E. Cassano, *J. Photochem. Photobiol., A*, 1993, **76**, 199.
36 H. Xu, W. Wang and W. Zhu, *J. Phys. Chem. B*, 2006, **110**, 13829.
37 X. Zhang, J. Song, J. Jiao and X. Mei, *Solid State Sci.*, 2010, **12**, 1215.
38 T. Ghodselahi, M. A. Vesaghi, A. Shafiekhani, A. Baghizadeh and M. Lameii, *Appl. Surf. Sci.*, 2008, **255**, 2730.
39 F. Shiraishi and C. Kawanishi, *J. Phys. Chem. A*, 2004, **108**, 10491.
40 W. Wang, L. Zhang, T. An, G. Li, H. Yip and P. Wong, *Appl. Catal., B*, 2011, **108–109**, 108.
41 L. Xiong, M. Ouyang, L. Yan, J. Li, M. Qiu and Y. Yu, *Chem. Lett.*, 2009, **38**, 1154.
42 P. E. De Jongh, D. Vanmaekelbergh and J. J. Kelly, *J. Electrochem. Soc.*, 2000, **147**, 486.
43 P. E. De Jongh, D. Vanmaekelbergh and J. J. Kelly, *Chem. Commun.*, 1999, 1069.
44 H. Lin, S. Liao and S. Hung, *J. Photochem. Photobiol., A*, 2005, **174**, 82.
45 Y. Zhang, L. Ma, J. Li and Y. Yu, *Environ. Sci. Technol.*, 2007, **41**, 6264.
46 M. Azami, M. Bahram, S. Nouri and A. Naseri, *J. Serb. Chem. Soc.*, 2012, **77**, 235.
47 H. Yang, K. Zhang, R. Shi, X. Li, X. Dong and Y. Yu, *J. Alloys Compd.*, 2006, **413**, 302.
48 H. K. Willem, M. S. David and L. B. Patricia, *Free Radical Biol. Med.*, 2010, **49**, 317.

